Combinatorial protein engineering of proteolytically resistant mesotrypsin inhibitors as candidates for cancer therapy

Itay Cohen[a], **Olumide Kayode**[b], **Alexandra Hockla**[b], **Banumathi Sankaran**[c], **Derek Radisky**[b], **Evette Radisky**[b,1], and **Niv Papo**[a,1]

[a]Department of Biotechnology Engineering and the National Institute of Biotechnology in the Negev, Ben-Gurion University of the Negev, Beer-Sheva, Israel

[b]Department of Cancer Biology, Mayo Clinic Comprehensive Cancer Center, Jacksonville, Florida 32224, USA

[c]Berkeley Center for Structural Biology, Lawrence Berkeley National Laboratory, Berkeley, California 94720, USA

Abstract

Engineered protein therapeutics offer advantages, including strong target affinity, selectivity, and low toxicity, but like natural proteins can be susceptible to proteolytic degradation, thereby limiting their effectiveness. A compelling therapeutic target is mesotrypsin, a protease upregulated with tumor progression, associated with poor prognosis, and implicated in tumor growth and progression of many cancers. However, with its unique capability for cleavage and inactivation of proteinaceous inhibitors, mesotrypsin presents a formidable challenge to the development of biologic inhibitors. We used a powerful yeast display platform for directed evolution, employing a novel multi-modal library screening strategy, to engineer the human amyloid precursor protein Kunitz protease inhibitor domain (APPI) simultaneously for increased proteolytic stability, stronger binding affinity, and improved selectivity for mesotrypsin inhibition. We identified a triple mutant APPI$_{M17G/I18F/F34V}$, with a mesotrypsin inhibition constant (K_i) of 89 pM, as the strongest mesotrypsin inhibitor yet reported; this variant displays 1459-fold improved affinity, up to 350,000-fold greater specificity, and 83-fold improved proteolytic stability vs wild-type APPI. We demonstrated that APPI$_{M17G/I18F/F34V}$ acts as a functional inhibitor in cell-based models of mesotrypsin-dependent prostate cancer cellular invasiveness. Additionally, by solving the crystal structure of the APPI$_{M17G/I18F/F34V}$/mesotrypsin complex, we obtained new insights into the structural and mechanistic basis for improved binding and proteolytic resistance. Our study identifies a promising mesotrypsin inhibitor as a starting point for development of anticancer protein therapeutics and establishes proof-of-principle for a novel library screening approach that will be widely applicable for simultaneously evolving proteolytic stability in tandem with desired functionality for diverse protein scaffolds.

CONFLICT OF INTEREST

The authors declare that they have no conflict of interest with respect to publication of this paper.

INTRODUCTION

The human serine protease mesotrypsin, encoded by the *PRSS3* gene, has recently emerged as a compelling new candidate drug target in cancer. Although its specific pathological roles are yet to be fully elucidated, the dysregulation and overexpression of mesotrypsin are associated with poor prognosis in many human tumors and with malignant behaviors in cancer models [1–9]. Mesotrypsin is particularly attractive as a potential target in the treatment of metastatic prostate cancer: it is associated with recurrence and metastasis and is upregulated in metastatic tumors. In cell culture and orthotopic mouse models, mesotrypsin drives invasive and metastatic phenotypes [2]. Likewise, in pancreatic cancer, higher mesotrypsin expression is associated with poorer patient survival, and in cell culture and animal models it promotes cancer cell proliferation, invasion, and metastasis [6]. Potent and selective inhibitors of mesotrypsin could thus offer both promise for the treatment of patients with aggressive metastatic cancers and tools to better dissect mesotrypsin function in cancer progression and metastasis.

Elucidating the mechanism of action of mesotrypsin and designing efficacious inhibitors are not trivial tasks [10–13]. A particular challenge in inhibitor development derives from the inability of mesotrypsin to form tight complexes with protein inhibitors, due to the presence of distinctive active site mutations [11, 13–15]. Furthermore, mesotrypsin also cleaves and inactivates many protein protease inhibitors as physiological substrates [12, 16, 17]. An additional challenge lies the inherent difficulty of obtaining selective inhibitors, since mesotrypsin shows high sequence homology and structural similarity with the major digestive trypsins (cationic and anionic trypsin) as well as with other serine proteases, including kallikreins and coagulation factors [18, 19]. It is thus not surprising that there are currently no effective inhibitory agents with high proteolytic stability, affinity and specificity for human mesotrypsin.

A conventional approach taken to developing inhibitors of other human serine proteases involves the engineering of natural serine protease inhibitors, such as those belonging to the Kunitz domain family [20–28]. These small proteins possess a protease-inhibitory binding loop of canonical conformation, supported by a compact scaffold with a three-dimensional structure that is maintained by hydrophobic packing and three disulfide bonds (Fig. S1C). From the perspective of developing selective drugs, the advantage of these inhibitors – over small molecules – is the availability of an extensive contact interface capable of interacting with multiple protease subsites. Initial attempts to engineer a potent polypeptide inhibitor of mesotrypsin by using bovine pancreatic trypsin inhibitor (BPTI) as a Kunitz domain scaffold that is relatively resistant to cleavage by mesotrypsin [29] revealed a number of drawbacks: BPTI exhibits a low affinity for mesotrypsin [15], a lack of target specificity [29], and a high potential for immune stimulation [30], and it may promote renal dysfunction [31]. Kunitz

domains of human origin are likely to be less immunogenic, but they are much more susceptible than BPTI to cleavage and inactivation by mesotrypsin [16, 17]. However, if such liabilities could be overcome, an engineered human Kunitz domain possessing mesotrypsin affinity, enhanced proteolytic stability, and target selectivity could offer a promising avenue for cancer therapy.

We thus pursued a novel combinatorial strategy to engineer the human Kunitz domain amyloid precursor protein inhibitor (APPI) simultaneously for increased proteolytic stability, higher binding affinity, and improved selectivity for inhibition of mesotrypsin. In light of our previous studies showing that the proteolytic stability of Kunitz domains is modulated by residues within the scaffold [32], we constructed an all-gene random mutagenesis APPI library in which diversity was introduced throughout the binding loop and the scaffold. Employing a stepwise proteolytic stability/affinity maturation process, we used yeast surface display (YSD) as a directed evolution methodology; this technique has previously been used to engineer proteins for enhanced binding affinity [33–35], proper folding [36, 37], and improved thermal stability [38].

Here, the YSD selection platform was applied for the first time to simultaneously screen for both proteolytic stability and affinity. High-throughput screening of tens of millions of yeast-displayed mutants enabled the rapid isolation of multiple APPI mutants, each carrying one mutation (either in the active site or in the scaffold) that individually conferred a functional enhancement in mesotrypsin affinity and/or proteolytic stability. By combining three mutations, we generated $APPI_{M17G/I18F/F34V}$, a triple mutant possessing the strongest affinity for mesotrypsin of any known inhibitor, with 1459-fold improved affinity and 83-fold improved proteolytic stability in comparison with wild-type APPI ($APPI_{WT}$). Remarkably, this triple mutant displayed 350,000-fold enhanced specificity toward mesotrypsin. We then demonstrated that these optimized properties enabled $APPI_{M17G/I18F/F34V}$ to potently block mesotrypsin-dependent cancer cell invasiveness in cell-based assays, for which high binding affinities and exceptional protease stabilities are crucial. In addition, by solving the crystal structure of the $APPI_{M17G/I18F/F34V}$/mesotrypsin complex, we revealed the molecular basis for the improved binding and proteolytic resistance of the engineered inhibitor as well as the basis for synergy between the mutations. Thus, our study establishes proof-of-principle for our novel multi-modal library screening approach. It also offers fundamental clues into the molecular basis of Kunitz domain stability and identifies a promising mesotrypsin inhibitor as a starting point for the development of anticancer protein therapeutics.

MATERIALS AND METHODS

Cells, reagents, and additional methods are described in *SI Materials and Methods*.

Generation of a combinatorial based APPI library

Synthesis and cloning of the DNA encoding $APPI_{WT}$ and the generation of the combinatorial APPI library are described in detail in *SI Materials and Methods*. In brief, the inhibitor domain of the amyloid precursor protein ($APPI_{WT}$) gene was constructed on the basis of a published sequence (PDB id 1ZJD) by using codons optimized for both *S.*

cerevisiae and *Pichia pastoris* usage and synthesized by PCR-assembly with six overlapping oligonucleotides. Next, a randomly mutated version of the APPI gene was constructed by error-prone PCR using nucleotide analogues and low-fidelity Taq polymerase with the APPI$_{WT}$ gene as a template. The resulting insert was amplified and transformed into yeast through homologous recombination, as previously described [39]. Random mutagenesis in the APPI sequence generated an APPI library with 0–3 mutations per clone, yielding an experimental library of about 9×10^6 clones.

Flow cytometry and cell sorting

The yeast-displayed APPI library and individual APPI variants were grown in SDCAA selective medium (as for SDCAA plates, but without agar; see *SI Materials and Methods*) and induced for expression with galactose medium (as for SDCAA, but with galactose instead of dextrose), according to established protocols [39]. Due to the different enzymatic turnover times of APPI and its variants by the target trypsins, i.e., bovine trypsin or mesotrypsin, two methods for trypsin-labeling were used, namely, 'double staining' and 'triple staining,' for the detection of proteolytically resistant clones, as described below. In the first step of labeling, approximately 1×10^6 cells were labeled with the appropriate catalytically active trypsin and a 1:50 dilution of mouse anti-c-Myc antibody in trypsin buffer (TB; 100 mM Tris-HCl, pH 8.0, 1 mM CaCl$_2$) supplemented with 1% bovine serum albumin (BSA) for 30 min at room temperature. In this labeling step, the cells were exposed to biotinylated-bovine trypsin or mesotrypsin for 'double staining.' For 'triple staining,' the cells were first treated with non-biotinylated mesotrypsin, and then an additional labelling step was applied: the cells were washed with TB and incubated with 2 μM of biotinylated catalytically inactive mesotrypsin-S195A for 1 h at room temperature. Finally, for both 'double staining' and 'triple staining,' cells were washed with ice-cold TB, followed by incubation with a 1:800 dilution of fluorescein isothiocyanate (FITC)-conjugated streptavidin and a 1:50 dilution of phycoerythrin (PE)-conjugated anti mouse secondary antibody for 30 min on ice. Cells were washed again and analyzed by dual-color flow cytometry (Accuri C6; BD Biosciences).

Cell sorting of 'triple-stained' cells was carried out as described in Figure 2A with a iCyt Synergy FACS [Cytometry, Proteomics and Microscopy Unit (CPMU), National Institute of Biotechnology in the Negev (NIBN), Ben-Gurion University of the Negev (BGU)]. In brief, approximately 1×10^8 cells were first sorted to select for high expressing clones (c-Myc clear). Sorted cells were then grown in selective medium, and several colonies were sequenced [DNA Microarray and Sequencing Unit (DMSU), NIBN, BGU]. Following each triple staining sort, the number of yeast cells used for subsequent sorting was at least 10-fold in excess of the number of sorted cells. Several clones from each round of sorting were sequenced. The concentration of the target protein in each sort is shown in Figure 2A.

Prostate cancer cell assays

Matrigel invasion assays of PC3-M human prostate cancer cells were conducted as previously reported [2]. Cells with *PRSS3* expression suppressed by lentiviral shRNA (NM_002771.2-454s1c1) served as a control in all experiments. Cells used for all other conditions were transduced with a control lentiviral shRNA that does not recognize any

human genes. Prior to the invasion assays, cells were seeded at 1.5×10^6 cells per 10 cm dish (day 1). Thereafter, the medium was replaced with a mixture of 3.6 ml RPMI containing 10% fetal bovine serum (FBS), 10 μg/ml Polybrene® and 2.4 ml conditioned medium containing lentiviral particles (day 2). The medium was replaced again after 24 h, and cells were selected with 2 μg/ml puromycin (day 3). On day 4, cells were trypsinized and seeded into 24-well 8.0 μm cell culture inserts (BD) previously coated with 50 μg Matrigel (2×10^4 cells per insert in 400 μl of medium). APPI$_{WT}$ or APPI$_{M17G/I18F/F34V}$ proteins (10 nM–1 μM) were added to cell suspensions in some wells as indicated in Figure 4A,B. Quadruple biological replicates were performed. Cells were allowed to invade toward a chemoattractant medium (750 μl NIH/3T3 cell-conditioned serum free medium) for 18 h, and then non-invading cells were removed, and the filters were fixed, stained and analyzed as described previously [2]. Consistent results were obtained from five independent experiments.

PC3-M cells for 3D culture assays were similarly transduced with either *PRSS3*-targeted or control lentiviral shRNA according to the above schedule. On day 4, cells were seeded into 3D cultures in Matrigel using the 'on-top' protocol, essentially as described previously [2, 40]. Briefly, in 12-well plates, a base layer of 250 μl of 100% Matrigel was polymerized, PC3-M cells (2×10^4 cells/well) were seeded and allowed to adhere to the substratum, excess medium was aspirated, and cells were overlaid with 500 μl of medium supplemented with 10% Matrigel and 0.5% FBS plus 100 nM of APPI$_{WT}$ or APPI$_{M17G/I18F/F34V}$ where indicated in Figure 4C,D. Cultures were maintained at 37 °C in 5% CO$_2$ for 3 d, photographed, and analyzed by counting and calculating the percentage of cells displaying spiky protrusions or branching morphology.

Protein complex crystallization, X-ray data collection, structure solution, and model refinement

APPI$_{M17G/I18F/F34V}$ was mixed with catalytically inactive mesotrypsin-S195A in an equimolar ratio at a total protein concentration of 4 mg/mL and then mixed 1:1 (v/v) with reservoir solution. The complex was crystallized at room temperature via the hanging drop method over a reservoir solution containing 0.1 M ammonium sulfate, 0.1 M Tris pH 7.5, and 20% PEG-1000. Crystals were harvested, cryoprotected, and flash cooled in liquid N$_2$. X-ray diffraction data were collected at 100 K, at beamline 8.2.1 of the Advanced Light Source, Lawrence Berkeley National Laboratory, from one crystal that diffracted to 1.83 Å. Data were merged and scaled with XDS [41]. The crystal belonged to the space group P4$_1$2$_1$2, with unit cell dimensions a = 78.15, b = 78.15, c = 243.73 and contained two copies of the complex in the asymmetric unit. The structure was solved by molecular replacement with MOLREP in CCP4 [42], using as the search model the complex of human mesotrypsin with APPI$_{WT}$ [Protein Data Bank (PDB) 3L33] [32]. Refinement employed alternating manual rebuilding in COOT [43] and automated refinement using REFMAC5 [44]. The quality of the final models was analyzed using wwPDB validation tools [45]. The coordinates and structure factors have been submitted to the Worldwide Protein Data Bank under the accession code 5C67.

RESULTS

Yeast-displayed APPI$_{WT}$ is rapidly cleaved by human mesotrypsin

The YSD system for directed evolution is based on the expression of a library of mutant proteins on the surface of yeast, followed by the selection of variants with improved affinity. However, this system has not been employed previously for identifying proteolytic cleavage or improving the proteolytic resistance of a displayed inhibitor. To test the compatibility of APPI$_{WT}$ with the YSD system, we cloned the coding region of APPI$_{WT}$ into a YSD plasmid for presentation on the *Saccharomyces cerevisiae* yeast surface as a fusion with the Aga2p agglutinin protein (Fig. S1). Correct folding of APPI$_{WT}$ was then verified by using flow activated cell sorting (FACS) for the detection of bound fluorescently labeled bovine trypsin, which is an established, tight-binding target of APPI [32]. We found that APPI displayed on the yeast surface was highly expressed and showed significant binding to bovine trypsin, thereby demonstrating proper folding of APPI (Figure 1A).

Next, we assessed the ability of mesotrypsin to detect APPI displayed on the yeast cell surface. Even with a broad range of mesotrypsin concentrations, we were not able to detect mesotrypsin binding (Figure 1B). We hypothesized that surface-displayed APPI is rapidly proteolysed by mesotrypsin, preventing detection of the transient binding event. This explanation is consistent with the previously reported rapid cleavage of APPI by mesotrypsin in solution (enzymatic turnover time of 24 s [16]) and with the relatively long incubation time (at least 60 min) required for cell labeling prior to FACS. We thus employed a catalytically inactive form of mesotrypsin, in which the serine nucleophile is mutated to alanine (mesotrypsin-S195A) (Figure 1C). Unlike active mesotrypsin, mesotrypsin-S195A bound to surface-displayed APPI and produced a strong FACS signal (Figure 1D, left panel). Additionally, we found that preincubation of APPI-displaying yeast cells with active mesotrypsin prior to detection with mesotrypsin-S195A resulted in a concentration-dependent decrease in the FACS signal (Figure 1D, right panels), thereby confirming our hypothesis that surface-displayed APPI is rapidly proteolysed and depleted by mesotrypsin.

Simultaneous affinity and proteolytic stability maturation of an APPI library

We next postulated that active mesotrypsin and mesotrypsin-S195A could be used in a stepwise fashion to enrich an APPI diversity library for variants with proteolytic resistance. As a starting point, we generated a randomized library in which mutations were introduced throughout the entire APPI gene at a frequency of 0–3 mutations per clone, producing a library of about 9×10^6 independent variants. Diversity was introduced throughout the molecule, because while protease specificity and affinity are largely directed by the sequence of the canonical binding loop, proteolytic stability is a property strongly influenced by residues within the scaffold, as we showed previously [32].

Our unique screening strategy, designated 'triple staining,' consisted of three steps (Figure 1C). First, active mesotrypsin was incubated with the yeast-displayed APPI library and allowed to cleave the less-resistant APPI clones. Second, active mesotrypsin was washed out and replaced with biotinylated mesotrypsin-S195A, which bound selectively to the uncleaved (resistant) clones. Third, the bound mesotrypsin-S195A was visualized by

staining with fluorescently labeled streptavidin, thereby facilitating detection. Elevated concentrations of active mesotrypsin were used as an evolutionary stimulus, with the fluorescently labeled mesotrypsin-S195A acting as a marker to facilitate identification of the most proteolytically resistant APPI variants (see 'triple staining' method, Figure 1C).

The initial library, termed S0 (where S stands for sort, and the number indicates the sort phase), was subjected to a round of expression enrichment based on c-Myc detection to yield the S1 library (Figure 2A, left plot). Subsequent rounds of affinity/stability maturation employed the 'triple staining' protocol. In sorting rounds S3, S4, and S5, diagonal sorting gates were used to select cell populations; this approach allowed binding normalization versus expression in real-time during the flow-cytometric sorting process, thereby dramatically decreasing bias of the expression level (i.e., the avidity effect) (Figure 2A).

'Triple staining' analysis of cells displaying $APPI_{WT}$ and cell populations from the library maturation cycles (S1 to S5) showed that the more advanced the sort, the higher the stability and affinity of the mutant library for mesotrypsin (Figure 2B). Remarkably, the S5 pool showed high tolerance to the proteolytic activity of mesotrypsin at all enzyme concentrations used. We then determined whether it would be possible to detect the binding interaction between active mesotrypsin and each of the sort generation clone pools (as was done with bovine trypsin). Indeed, 'double staining' analysis with FITC-labeled active mesotrypsin showed high binding in pools derived from the advanced sorting rounds (S4 and S5; Figure 2C). These results suggest a high representation of proteolytically resistant APPI variants in the S5 pool of stability-matured variants.

Identification of surface displayed APPI clones with improved mesotrypsin affinity and resistance to cleavage

DNA sequencing of 37 randomly selected APPI clones from S5 showed three repeating mutations, M17A, I18F, and F34V, along with a number of unique mutations (Table S1). In a previous rational mutagenesis study, we had identified M17A as a mutation mediating improved mesotrypsin affinity and resistance to cleavage and had also found that Gly at the same position conferred an even greater improvement [29]. Accordingly, we chose M17G to replace M17A for subsequent analysis of single and composite mutants.

Staining of the individual YSD clones with active mesotrypsin showed that M17G and I18F exhibited high binding affinity and proteolytic stability, whereas F34V had only marginally enhanced binding affinity and stability vs. $APPI_{WT}$ (Figure 2D). The three mutations are spatially close to each other in the three-dimensional structure of APPI and may be expected to interact physically. To better understand the potential functional interactions between the mutations, we investigated the effect of all possible combinations (Figure 2D), which allowed us to assess additive, cooperative (beneficial dependence), or uncooperative (harmful dependence) interactions between mutations with respect to affinity and proteolytic resistance. Importantly, the results imply an additive or cooperative effect, in which the triple mutant showed remarkably higher binding affinity and proteolytic stability than the other combinations.

Affinity/stability-matured APPI variants show improved mesotrypsin inhibition in solution

To accurately assess mesotrypsin affinity and proteolytic stability independently, we expressed and purified soluble forms of the mutant proteins (Fig. S2, S3 and S4). Correct folding (Fig. S5) and high thermostability (Fig. S5 and S6) were observed for all proteins [using circular dichroism (CD)]. Thereafter, we determined the inhibition constants (K_i) (see *SI*; eqn 1), approximating the enzyme-inhibitor dissociation constants, by testing APPI$_{WT}$ and mutated variants as inhibitors of mesotrypsin catalytic activity against the small chromogenic peptide substrate Z-GPR-pNA.

We observed a classic competition pattern of inhibition for all inhibitors (Figure 3A and B and Fig. S7*A–D*) and obtained a K_i value for APPI$_{WT}$ of 131 ± 17 nM (Table 1), consistent with previous work [16]. APPI$_{M17G}$ showed a ~40-fold improvement in K_i, as previously reported [29], and APPI$_{I18F}$ showed a similar improvement, whereas APPI$_{F34V}$ showed a ~threefold improvement in mesotrypsin affinity (Table 1).

Since the lowest K_i values of our single-mutation APPI variants were in the lower nanomolar range, close to the practical limit of determination using the classical competitive inhibition equation in our assay, it was not possible to apply this method for combination variants with lower K_i values. Therefore, an alternative kinetic treatment, suitable for the quantification of slow, tight binding behavior (see *SI*; Eq. 2) was thus used, as shown in Figure 3C–F and Fig. S7*F–J* and summarized in Table 1.

To compare the results obtained from the slow-tight binding *vs.* the classical competitive inhibition studies, APPI$_{M17G}$ inhibition was evaluated using both approaches, with the results showing a high correlation between the two methods (Figure 3A–D and Table 1). As anticipated, the K_i values for double and triple mutants were, for the most part, significantly enhanced vis-à-vis those for the single mutants (Table 1). In particular, we observed an outstanding improvement in binding – of more than three orders of magnitude – of our triple mutant variant ($K_i = 89.8$ pM) *vs.* the wild type ($K_i = 131,000$ pM) (Figure 3E and F and Table 1).

Affinity/stability-matured APPI variants show marked enhancement in proteolytic resistance in solution

To evaluate whether our 'stability maturation' strategy did indeed produce variants with improved proteolytic resistance towards mesotrypsin, we directly measured rates of inhibitor cleavage by mesotrypsin in HPLC-based time course hydrolysis assays. Because the proteolysis reactions were conducted at APPI variant concentrations far above their measured K_i values (which also represent K_m values for cleavage of the APPI variants as mesotrypsin substrates), the observed hydrolysis rates represent the catalytic rate constants (k_{cat}). The individual mutations resulting from the stability maturation process gave modestly improved (two- to fourfold) proteolytic stability (Table 1). Pairs of mutations resulted in greater improvements (6- to 12-fold), while the APPI$_{M17G/I18F/F34V}$ triple mutant displayed a remarkable 83-fold improvement in proteolytic resistance towards mesotrypsin (Figure 3G,H, Fig. S8 and Table 1).

Most importantly, when combined to form the $APPI_{M17G/I18F/F34V}$ triple mutant, the three mutations (M17G, I18F, and F34V) act cooperatively in most cases with respect to affinity and in all cases with respect to proteolytic stability (See *SI*).

To test the specificity of the $APPI_{M17G/I18F/F34V}$ triple mutant, we selected cationic trypsin, anionic trypsin, factor XIa (FXIa) and kallikrein-6 [46] as targets that bind tightly to $APPI_{WT}$ and therefore serve as competitors for *in vivo* mesotrypsin binding. Importantly, we found that while $APPI_{M17G/I18F/F34V}$ showed greatly improved binding affinity toward mesotrypsin vis-à-vis $APPI_{WT}$, affinity improvements toward kallikrein-6 and cationic and anionic trypsins were negligible, and affinity was substantially weakened toward the APPI physiological target FXIa. Thus, the mutations present in $APPI_{M17G/I18F/F34V}$ result in enhancement of specificity toward mesotrypsin over other proteases by three to five orders of magnitude (Table 2). These results suggest that $APPI_{M17G/I18F/F34V}$ may indeed constitute a suitable candidate for *in vivo* applications targeting mesotrypsin.

$APPI_{M17G/I18F/F34V}$ variant reveals enhanced potency for inhibition of mesotrypsin-dependent cancer cell invasiveness

To evaluate the ability of the $APPI_{M17G/I18F/F34V}$ triple mutant to inhibit invasive behavior, we used human PC3-M cells, a hormone-independent, highly aggressive and metastatic prostate cancer cell line [47]. Matrigel invasion assays confirmed that mesotrypsin expression is essential for the invasiveness of these cells, since transduction with a lentiviral shRNA construct targeting the *PRSS3* gene resulted in profound inhibition of cells passing through the membrane barrier (Figure 4A,B, KD control), as previously reported [2]. When control cells with endogenous *PRSS3* expression were treated with 10 nM $APPI_{M17G/I18F/F34V}$, significant inhibition of invasion was observed, whereas 10 nM $APPI_{WT}$ did not produce a significant effect. At much higher inhibitor concentrations (1 μM), both inhibitors produced similar maximum inhibitory effects of ~50%.

To further explore the impact of APPI-based inhibitors on prostate cancer cells in a physiologically relevant environment, we grew PC3-M cells in 3D Matrigel culture. As reported previously [2], these cells displayed a native growth morphology characterized by spiky protrusions when grown in 3D (Figure 4C, upper left panel). Lentiviral shRNA silencing of *PRSS3* significantly reduced the proportion of cells displaying this invasive morphology, as did treatment of the cultures with 100 nM $APPI_{M17G/I18F/F34V}$ (Figure 4C,D). In contrast, treatment of cells with $APPI_{WT}$ at the same concentration did not produce a comparable effect (Figure 4C,D). Taken together, these experiments demonstrate the enhanced potency of $APPI_{M17G/I18F/F34V}$ compared to $APPI_{WT}$ for suppression of cellular invasiveness. The inability of either $APPI_{WT}$ or $APPI_{M17G/I18F/F34V}$ to suppress invasion or invasive morphology to the same extent as mesotrypsin knockdown may result from inadequate selectivity or from competition for binding from other proteases in the cellular milieu; this possibility reinforces the necessity for continued engineering efforts to further enhance the selectivity of mesotrypsin-targeted APPI variants.

High-resolution crystal structure of APPI$_{M17G/I18F/F34V}$ bound to mesotrypsin provides insight into functional improvements

To gain insight into the mechanistic basis for improved mesotrypsin affinity and resistance to proteolysis of APPI$_{M17G/I18F/F34V}$, we co-crystallized the inhibitor with mesotrypsin and solved and refined the structure of the complex at 1.83 Å resolution (Table S2). Overall, the structure is highly similar to the previously-solved APPI$_{WT}$ complex with mesotrypsin [PDB ID: 3L33; [32]], including similar disulfide bond topology of the inhibitor. Mutations at APPI residues 17 and 18, located on the primed side of the canonical binding loop, altered enzyme-inhibitor interactions in the S$_2'$ and S$_3'$ subsites. The mesotrypsin S$_2'$ subsite is defined by the atypical Arg-193 residue (a highly conserved Gly in other trypsins), responsible for steric interactions that disfavor bulky P$_2'$ substrate or inhibitor residues [29]. Arg-193 has been found to adopt multiple conformations depending on the P$_2'$ residue of a bound inhibitor [17, 29]. In the structure of mesotrypsin bound to APPI$_{WT}$ [PDB ID: 3L33; [32]], Arg-193 is pushed upward by the inhibitor P$_2'$ residue Met-17 into a cleft between the two beta-barrels of mesotrypsin (Figure 5A). The mutation of APPI Met-17 to Gly removes constraints on the conformation of Arg-193 in the complex, and, intriguingly, Arg-193 adopts different conformations in the two copies of the complex in our new crystal structure (Figure 5B). One conformation is similar to the 'up' conformation observed in the APPI$_{WT}$ complex structure, while the other is similar to the 'down' conformation previously seen in structures of mesotrypsin bound to the small molecule inhibitor benzamidine [PDB ID: 1H4W; [13]] or to mutant BPTI possessing Gly at the P$_2'$ position [PDB ID:3P92; [29]]. The observation of both Arg-193 conformations within the same crystal reveals that these conformations are roughly energetically equivalent and suggests that the improved affinity attributable to Gly-17 may result, at least in part, from preservation of conformational entropy in the vicinity of Arg-193 upon binding. The elimination of unfavorable steric interactions between Arg-193 and Met-17 (as found in APPI$_{WT}$) [29, 32] may additionally contribute to the improved mesotrypsin affinity of variants possessing Gly-17.

The mutation of APPI Ile-18 to Phe optimizes intermolecular packing in the S$_3'$ subsite, resulting in the formation of new van der Waals forces, ring-stacking and hydrophobic contacts with Phe-41 and Lys-60 of mesotrypsin (Figure 6). The closest interatomic distance between the aromatic rings of APPI Phe-18 and mesotrypsin Phe-41 is 3.5 Å, which is consistent with the 3.8 Å that is typical of stabilizing aromatic pairs within proteins [48, 49]. The APPI Phe-18 aromatic ring is also located within 5 Å of the N$_\zeta$ atom of mesotrypsin Lys-60, suggesting that favorable amino-aromatic interactions [50] may also potentially contribute to the enhancement of binding affinity. Taken together, these interactions enhance affinity by providing energetically favorable contacts between the enzyme and inhibitor, which are absent in the wild-type APPI-mesotrypsin complex.

The mutation of Phe-34 to Val in APPI is located within the inhibitor scaffold, rather than in the canonical binding loop (Figure 7A). The Val-34 side chain approaches within 3.7 Å of the hydroxyl group of mesotrypsin Tyr-151 but otherwise does not make close contact with the enzyme. Residues 34 and 17 lie adjacent in the Kunitz domain structure, and the side chain of residue 34 constrains the conformation and mobility of residue 17. Val-34 C$_{\gamma1}$ forms a close contact of 3.5 Å with Gly-17 C$_\alpha$, which is not present in APPI$_{WT}$ (Figure

7A,B); the resulting tighter intramolecular packing within $APPI_{M17G/I18F/F34V}$ potentially imposes greater constraints on the backbone mobility of residue 17. Consistent with this observation, the positive cooperativity of M17G and F34V seen in analyses of affinity improvements, proteolytic resistance, and energetic additivity (Table 1 and Fig. S9) suggests the possibility that the major importance of Val-34 may lie in its influence on the conformation and dynamics of Gly-17. Comparison of the structures of $APPI_{WT}$ and $APPI_{M17G/I18F/F34V}$ additionally reveals subtle backbone shifts of up to ~1 Å that enable the formation in the triple mutant of a new hydrogen bond between the carbonyl oxygen of Val-34 and the hydroxyl of Thr-11 (Figure 7A,B). This H bond, absent in most structures of $APPI_{WT}$ but present in all structures of BPTI, may confer additional rigidity on the inhibitor scaffold and hence contribute to proteolytic stability.

DISCUSSION

During the past decade, mesotrypsin has emerged as a significant player in different stages of cancer development, being associated with cell malignancy in multiple cancers, including lung, colon, breast, pancreas and prostate cancers [1–6]. These studies have implicated mesotrypsin as a potential new therapeutic target. In the present study, we have identified a novel inhibitor with an unprecedented combination of mesotrypsin affinity, proteolytic stability, and biological potency, offering promise for development of new therapeutics.

Early studies of transendothelial migration in non-small cell lung cancer (NSCLC) cultures showed mesotrypsin overexpression to be associated with invasion and metastasis, while comparative microarray assays of cells taken from NSCLC patients showed mesotrypsin overexpression to be predictive of poor survival [1]. The first report to offer some mechanistic insight into the putative role of mesotrypsin in cancer progression showed a correlation between the upregulation of mesotrypsin and malignant progression in a breast cancer cell line. In that study, it was found that CD109, a cell-surface glycoprotein, acts as a potential mesotrypsin substrate involved in driving malignancy [5]. An indirect tumorigenic effect (in pancreatic cancer cells) – mediated by upregulation of VEGF expression – via the protease-activated receptor1 (PAR1)-mediated ERK pathway has also been suggested for mesotrypsin [6]. A more direct, and specific, role for the proteolytic activity of mesotrypsin in cancer cell invasiveness was recently described for metastatic prostate tumors [2]. While treatment with mesotrypsin directly promoted an invasive cellular phenotype, neither cationic trypsin nor a non-catalytic mesotrypsin variant could similarly drive this invasive phenotype, suggesting that the promotion of invasion depends on the specific proteolytic activity of mesotrypsin [2]. Indeed, a clue to the role played by mesotrypsin in metastasis may be found in the enhanced catalytic capability of mesotrypsin to hydrolyze canonical trypsin inhibitors that are highly abundant in the tumor microenvironment, such as human Kunitz protease inhibitor domains from amyloid precursor-like protein 2 (APLP2), bikunin, hepatocyte growth factor activator inhibitor type 2 (HAI2) and others [16, 17]. Cleavage and inactivation of these inhibitors as physiological substrates by mesotrypsin may plausibly contribute to its significant role in the mechanism of metastasis enhancement [16, 17]. In the present work, we have engineered a human Kunitz domain inhibitor that is remarkably resistant to mesotrypsin proteolysis, which we expect will block mesotrypsin's metastasis-promoting activity.

Although mesotrypsin and other trypsins share many residues that contribute to similar primary specificity, mesotrypsin exhibits unique sequence and structural features that are responsible for its enhanced catalytic capability and distinct resistance towards canonical trypsin inhibitors. This resistance is most notably the result of two evolutionary mutations in mesotrypsin: the substitution of Gly-193 by Arg, which clashes sterically with the inhibitors, and the substitution of Tyr-39 by Ser, which prevents the formation of a hydrogen bond within the mesotrypsin/inhibitor complexes [[11], 14, 15]. These mutations are thus responsible for the unusually low affinity of mesotrypsin (relative to typical trypsins) for polypeptide trypsin inhibitors, and also contribute to the more surprising ability of mesotrypsin to cleave several canonical trypsin inhibitors as substrates [12, 16, 17]. Additional unique mesotrypsin residues, Lys-74 and Asp-97, located on the periphery of the active site, have further evolutionarily adapted mesotrypsin for efficient cleavage of trypsin inhibitors [14]. The net effect of these evolutionary adaptations is to weaken favorable interactions, promote unfavorable interactions, and enhance protein dynamics at the interface between mesotrypsin and a bound canonical trypsin inhibitor [11, 14, 15]. Since the rate-limiting step in canonical inhibitor proteolysis is attributed to the hydrolysis of the acyl enzyme (requiring dissociation of the primed side residues of the canonical binding loop from the enzyme's active site) [51], the weakened association and enhanced dynamics present in mesotrypsin-inhibitor complexes are expected to result in more rapid deacylation and expulsion of the cleaved inhibitor from the active site.

Notably, we found that the combination of three mutations in $APPI_{M17G/I18F/F34V}$ produces a mesotrypsin-inhibitor complex featuring a much more complementary binding interface, at which new favorable interactions of the inhibitor with mesotrypsin S_2' and S_3' subsites are exhibited on the primed side of the active site (Figures 6, 7); this explains the improved affinity of $APPI_{M17G/I18F/F34V}$ for mesotrypsin. To the extent that these favorable interactions are maintained during catalysis and following inhibitor cleavage, they may be expected to retard the dissociation of the cleaved inhibitor from the active site, thus contributing to the markedly improved stability of $APPI_{M17G/I18F/F34V}$ to proteolysis by mesotrypsin. The $APPI_{M17G/I18F/F34V}$ structure also revealed new stabilizing intramolecular features within the inhibitor scaffold (Figure 7); these may dampen the conformational dynamics of the molecule, thus further retarding proteolysis. The functional cooperativity between the three mutated residues, evident in our analyses of free energy additivity (Fig. S9), appears to be quite complex, and perhaps cannot be fully understood from the crystal structure alone, in the absence of data to describe the impact of the mutations on protein dynamics. Nonetheless, based on the crystal structure, we suggest that the intimate packing between Val-34 and Gly-17 (Figure 7) may synergistically stabilize inhibitor scaffold-binding loop interactions and thus slow proteolysis. Gly-17 and Phe-18 each independently enhance affinity for the enzyme and, by slowing dissociation of primed-side residues from the enzyme, also retard proteolysis. However, it appears that only in the triple mutant is there full optimization of both intramolecular packing within the inhibitor and intermolecular packing with the enzyme, resulting in greater cooperative enhancements in both affinity and proteolytic resistance.

While the capacity of mesotrypsin to cleave inhibitors presents a challenge from the perspective of inhibitor development, once a protein scaffold has been sufficiently stabilized

to resist mesotrypsin cleavage, these very same distinctive active site features may provide an opportunity to develop mesotrypsin-selective inhibitors that can be exploited for therapeutic and diagnostic purposes. Our prior attempts to develop peptide-based mesotrypsin inhibitors using a structure-guided rational mutagenesis approach [29, 32] have demonstrated that mesotrypsin affinity is largely modulated by specific residues within the inhibitor binding loop, whereas inhibitor stability to mesotrypsin hydrolysis is highly influenced by scaffold residues. While the contributions of several binding loop residues to affinity have been previously identified [29, 32], the specific scaffold residues that contribute to proteolytic resistance have remained obscure until now. In this study, we have taken an unbiased combinatorial directed evolution approach – incorporating diversity throughout both the binding loop and scaffold – enhanced by a unique "triple staining" screening strategy, to enable, for the first time, simultaneous evolution of proteolytic stability and affinity. Intriguingly, our screening identified both binding loop and scaffold residues that acted cooperatively to enhance both mesotrypsin affinity and proteolytic stability. The best mesotrypsin inhibitor that we identified using this approach exhibited both 1459-fold higher affinity and 83-fold greater proteolytic stability than the parent molecule, making it by far the most potent inhibitor of mesotrypsin reported to date. Importantly, this novel inhibitor also reduced cellular invasion at nanomolar concentrations in cell-based assays (Figure 4), thus showing promise for development as a therapeutic or diagnostic agent. We anticipate that continued engineering efforts using this platform and screening strategy may further enhance the selectivity of mesotrypsin-targeted APPI variants, providing improved efficacy in the cellular context.

In conclusion, mesotrypsin has recently been identified as a protease that is upregulated in concert with tumor progression in many different high incidence and poor prognosis cancers. It has been found that silencing of mesotrypsin expression can inhibit cancer growth, invasion, and metastasis in cell culture and in mouse models, thus implicating mesotrypsin as a putative therapeutic target. However, it has proved difficult to engineer mesotrypsin inhibitors that possess high affinity and proteolytic stability. This study demonstrates that APPI provides a suitable protein scaffold for developing mesotrypsin inhibitors and that the YSD platform in concert with our unique screening approach offers a powerful method to simultaneously engineer proteolytic resistance, affinity and specificity. Such novel inhibitors will offer promising avenues for cancer therapy and imaging applications; they will also constitute extremely valuable laboratory reagents for deciphering the specific mechanisms by which mesotrypsin drives cancer progression. Finally, as proteolytic degradation is a general challenge faced in development of protein therapeutics, we suggest that similar YSD screening strategies employing active protease exposure as evolutionary stimuli may have wide applicability to the development of diverse protein-based drugs and diagnostics for many applications.

Supplementary Material

Refer to Web version on PubMed Central for supplementary material.

Acknowledgments

Abbreviations

APPI	amyloid precursor protein Kunitz protease inhibitor domain
BGU	Ben-Gurion University of the Negev
BPTI	bovine pancreatic trypsin inhibitor
BSA	bovine serum albumin
CD	circular dichroism
CPMU	Cytometry, Proteomics and Microscopy Unit
DMSU	DNA Microarray and Sequencing Unit
FACS	flow activated cell sorting
FBS	fetal bovine serum
FITC	fluorescein isothiocyanate
FXIa	factor XIa
KD	knockdown
NIBN	National Institute of Biotechnology in the Negev
NSCLC	non-small cell lung cancer
PE	phycoerythrin
TB	trypsin buffer
YSD	yeast surface display

References

1. Diederichs S, Bulk E, Steffen B, Ji P, Tickenbrock L, Lang K, Zanker KS, Metzger R, Schneider PM, Gerke V, et al. S100 family members and trypsinogens are predictors of distant metastasis and survival in early-stage non-small cell lung cancer. Cancer Res. 2004; 64:5564–5569. [PubMed: 15313892]

2. Hockla A, Miller E, Salameh MA, Copland JA, Radisky DC, Radisky ES. PRSS3/mesotrypsin is a therapeutic target for metastatic prostate cancer. Mol Cancer Res. 2012; 10:1555–1566. [PubMed: 23258495]

3. Yang L, Zhang L, Wu Q, Boyd DD. Unbiased screening for transcriptional targets of ZKSCAN3 identifies integrin beta 4 and vascular endothelial growth factor as downstream targets. J Biol Chem. 2008; 283:35295–35304. [PubMed: 18940803]

4. Dozmorov MG, Hurst RE, Culkin DJ, Kropp BP, Frank MB, Osban J, Penning TM, Lin HK. Unique patterns of molecular profiling between human prostate cancer LNCaP and PC-3 cells. Prostate. 2009; 69:1077–1090. [PubMed: 19343732]

5. Hockla A, Radisky DC, Radisky ES. Mesotrypsin promotes malignant growth of breast cancer cells through shedding of CD109. Breast Cancer Res Treat. 2010; 124:27–38. [PubMed: 20035377]

6. Jiang G, Cao F, Ren G, Gao D, Bhakta V, Zhang Y, Cao H, Dong Z, Zang W, Zhang S, et al. PRSS3 promotes tumour growth and metastasis of human pancreatic cancer. Gut. 2010; 59:1535–1544. [PubMed: 20947888]

7. Ghilardi C, Silini A, Figini S, Anastasia A, Lupi M, Fruscio R, Giavazzi R, Bani M. Trypsinogen 4 boosts tumor endothelial cells migration through proteolysis of tissue factor pathway inhibitor-2. Oncotarget. 2015

8. Ma R, Ye X, Cheng H, Ma Y, Cui H, Chang X. PRSS3 expression is associated with tumor progression and poor prognosis in epithelial ovarian cancer. Gynecologic oncology. 2015; 137:546–552. [PubMed: 25735255]

9. Han S, Lee CW, Trevino JG, Hughes SJ, Sarosi GA Jr. Autocrine extra-pancreatic trypsin 3 secretion promotes cell proliferation and survival in esophageal adenocarcinoma. PloS one. 2013; 8:e76667. [PubMed: 24146905]

10. Salameh MA, Radisky ES. Biochemical and structural insights into mesotrypsin: an unusual human trypsin. Int J Biochem Mol Biol. 2013; 4:129–139. [PubMed: 24049668]

11. Salameh MA, Soares AS, Alloy A, Radisky ES. Presence versus absence of hydrogen bond donor Tyr-39 influences interactions of cationic trypsin and mesotrypsin with protein protease inhibitors. Protein Sci. 2012; 21:1103–1112. [PubMed: 22610453]

12. Szmola R, Kukor Z, Sahin-Toth M. Human mesotrypsin is a unique digestive protease specialized for the degradation of trypsin inhibitors. J Biol Chem. 2003; 278:48580–48589. [PubMed: 14507909]

13. Katona G, Berglund GI, Hajdu J, Graf L, Szilagyi L. Crystal structure reveals basis for the inhibitor resistance of human brain trypsin. J Mol Biol. 2002; 315:1209–1218. [PubMed: 11827488]

14. Alloy AP, Kayode O, Wang R, Hockla A, Soares AS, Radisky ES. Mesotrypsin Has Evolved Four Unique Residues to Cleave Trypsin Inhibitors as Substrates. J Biol Chem. 2015; 290:21523–21535. [PubMed: 26175157]

15. Salameh MA, Soares AS, Hockla A, Radisky ES. Structural basis for accelerated cleavage of bovine pancreatic trypsin inhibitor (BPTI) by human mesotrypsin. J Biol Chem. 2008; 283:4115–4123. [PubMed: 18077447]

16. Salameh MA, Robinson JL, Navaneetham D, Sinha D, Madden BJ, Walsh PN, Radisky ES. The amyloid precursor protein/protease nexin 2 Kunitz inhibitor domain is a highly specific substrate of mesotrypsin. J Biol Chem. 2010; 285:1939–1949. [PubMed: 19920152]

17. Pendlebury D, Wang R, Henin RD, Hockla A, Soares AS, Madden BJ, Kazanov MD, Radisky ES. Sequence and conformational specificity in substrate recognition: several human Kunitz protease inhibitor domains are specific substrates of mesotrypsin. J Biol Chem. 2014; 289:32783–32797. [PubMed: 25301953]

18. Emi M, Nakamura Y, Ogawa M, Yamamoto T, Nishide T, Mori T, Matsubara K. Cloning, characterization and nucleotide sequences of two cDNAs encoding human pancreatic trypsinogens. Gene. 1986; 41:305–310. [PubMed: 3011602]

19. Wiegand U, Corbach S, Minn A, Kang J, Muller-Hill B. Cloning of the cDNA encoding human brain trypsinogen and characterization of its product. Gene. 1993; 136:167–175. [PubMed: 8294000]

20. Dennis MS, Herzka A, Lazarus RA. Potent and selective Kunitz domain inhibitors of plasma kallikrein designed by phage display. J Biol Chem. 1995; 270:25411–25417. [PubMed: 7592708]

21. Dennis MS, Lazarus RA. Kunitz domain inhibitors of tissue factor-factor VIIa. II. Potent and specific inhibitors by competitive phage selection. J Biol Chem. 1994; 269:22137–22144. [PubMed: 8071338]

22. Dennis MS, Lazarus RA. Kunitz domain inhibitors of tissue factor-factor VIIa. I. Potent inhibitors selected from libraries by phage display. J Biol Chem. 1994; 269:22129–22136. [PubMed: 8071337]

23. Markland W, Ley AC, Ladner RC. Iterative optimization of high-affinity protease inhibitors using phage display. 2. Plasma kallikrein and thrombin. Biochemistry. 1996; 35:8058–8067. [PubMed: 8672510]

24. Markland W, Ley AC, Lee SW, Ladner RC. Iterative optimization of high-affinity proteases inhibitors using phage display. 1. Plasmin. Biochemistry. 1996; 35:8045–8057. [PubMed: 8672509]

25. Roberts BL, Markland W, Ley AC, Kent RB, White DW, Guterman SK, Ladner RC. Directed evolution of a protein: selection of potent neutrophil elastase inhibitors displayed on M13 fusion phage. Proc Natl Acad Sci U S A. 1992; 89:2429–2433. [PubMed: 1549606]

26. Li W, Wang BE, Moran P, Lipari T, Ganesan R, Corpuz R, Ludlam MJ, Gogineni A, Koeppen H, Bunting S, et al. Pegylated kunitz domain inhibitor suppresses hepsin-mediated invasive tumor growth and metastasis. Cancer Res. 2009; 69:8395–8402. [PubMed: 19843851]

27. Devy L, Rabbani SA, Stochl M, Ruskowski M, Mackie I, Naa L, Toews M, van Gool R, Chen J, Ley A, et al. PEGylated DX-1000: pharmacokinetics and antineoplastic activity of a specific plasmin inhibitor. Neoplasia. 2007; 9:927–937. [PubMed: 18030361]

28. Williams A, Baird LG. DX-88 and HAE: a developmental perspective. Transfusion and apheresis science : official journal of the World Apheresis Association : official journal of the European Society for Haemapheresis. 2003; 29:255–258.

29. Salameh MA, Soares AS, Hockla A, Radisky DC, Radisky ES. The P(2)′ residue is a key determinant of mesotrypsin specificity: engineering a high-affinity inhibitor with anticancer activity. Biochem J. 2011; 440:95–105. [PubMed: 21806544]

30. Fioretti E, Angeletti M, Citro G, Barra D, Ascoli F. Kunitz-type inhibitors in human serum. Identification and characterization. J Biol Chem. 1987; 262:3586–3589. [PubMed: 3546310]

31. Bajaj MS, Ogueli GI, Kumar Y, Vadivel K, Lawson G, Shanker S, Schmidt AE, Bajaj SP. Engineering kunitz domain 1 (KD1) of human tissue factor pathway inhibitor-2 to selectively inhibit fibrinolysis: properties of KD1-L17R variant. J Biol Chem. 2011; 286:4329–4340. [PubMed: 21115497]

32. Salameh MA, Soares AS, Navaneetham D, Sinha D, Walsh PN, Radisky ES. Determinants of affinity and proteolytic stability in interactions of Kunitz family protease inhibitors with mesotrypsin. J Biol Chem. 2010; 285:36884–36896. [PubMed: 20861008]

33. Graff CP, Chester K, Begent R, Wittrup KD. Directed evolution of an anti-carcinoembryonic antigen scFv with a 4-day monovalent dissociation half-time at 37 degrees C. Protein Eng Des Sel. 2004; 17:293–304. [PubMed: 15115853]

34. Boder ET, Wittrup KD. Yeast surface display for screening combinatorial polypeptide libraries. Nat Biotechnol. 1997; 15:553–557. [PubMed: 9181578]

35. Boder ET, Midelfort KS, Wittrup KD. Directed evolution of antibody fragments with monovalent femtomolar antigen-binding affinity. Proc Natl Acad Sci U S A. 2000; 97:10701–10705. [PubMed: 10984501]

36. Kim YS, Bhandari R, Cochran JR, Kuriyan J, Wittrup KD. Directed evolution of the epidermal growth factor receptor extracellular domain for expression in yeast. Proteins. 2006; 62:1026–1035. [PubMed: 16355407]

37. Kieke MC, Shusta EV, Boder ET, Teyton L, Wittrup KD, Kranz DM. Selection of functional T cell receptor mutants from a yeast surface-display library. Proc Natl Acad Sci U S A. 1999; 96:5651–5656. [PubMed: 10318939]

38. Shusta EV, Holler PD, Kieke MC, Kranz DM, Wittrup KD. Directed evolution of a stable scaffold for T-cell receptor engineering. Nat Biotechnol. 2000; 18:754–759. [PubMed: 10888844]

39. Chao G, Lau WL, Hackel BJ, Sazinsky SL, Lippow SM, Wittrup KD. Isolating and engineering human antibodies using yeast surface display. Nat Protoc. 2006; 1:755–768. [PubMed: 17406305]

40. Lee GY, Kenny PA, Lee EH, Bissell MJ. Three-dimensional culture models of normal and malignant breast epithelial cells. Nature methods. 2007; 4:359–365. [PubMed: 17396127]

41. Kabsch W. Xds. Acta Crystallogr D Biol Crystallogr. 2010; 66:125–132. [PubMed: 20124692]

42. Vagin A, Teplyakov A. Molecular replacement with MOLREP. Acta Crystallogr D Biol Crystallogr. 2010; 66:22–25. [PubMed: 20057045]

43. Emsley P, Cowtan K. Coot: model-building tools for molecular graphics. Acta Crystallographica Section D: Biological Crystallography. 2004; 60:2126–2132. [PubMed: 15572765]

44. Murshudov GN, Vagin AA, Dodson EJ. Refinement of macromolecular structures by the maximum-likelihood method. Acta Crystallographica Section D: Biological Crystallography. 1997; 53:240–255. [PubMed: 15299926]

45. Read RJ, Adams PD, Arendall WB 3rd, Brunger AT, Emsley P, Joosten RP, Kleywegt GJ, Krissinel EB, Lutteke T, Otwinowski Z, et al. A new generation of crystallographic validation tools for the protein data bank. Structure. 2011; 19:1395–1412. [PubMed: 22000512]

46. Navaneetham D, Sinha D, Walsh PN. Mechanisms and specificity of factor XIa and trypsin inhibition by protease nexin 2 and basic pancreatic trypsin inhibitor. J Biochem. 2010; 148:467–479. [PubMed: 20647553]

47. Kozlowski JM, Fidler IJ, Campbell D, Xu ZL, Kaighn ME, Hart IR. Metastatic behavior of human tumor cell lines grown in the nude mouse. Cancer Res. 1984; 44:3522–3529. [PubMed: 6744277]

48. McGaughey GB, Gagne M, Rappe AK. pi-Stacking interactions. Alive and well in proteins. J Biol Chem. 1998; 273:15458–15463. [PubMed: 9624131]

49. Thomas A, Meurisse R, Charloteaux B, Brasseur R. Aromatic side-chain interactions in proteins. I. Main structural features. Proteins. 2002; 48:628–634. [PubMed: 12211030]

50. Burley SK, Petsko GA. Amino-aromatic interactions in proteins. FEBS Lett. 1986; 203:139–143. [PubMed: 3089835]

51. Radisky ES, Koshland DE Jr. A clogged gutter mechanism for protease inhibitors. Proc Natl Acad Sci U S A. 2002; 99:10316–10321. [PubMed: 12142461]

52. Wilson DS, Keefe AD. Random mutagenesis by PCR. Curr Protoc Mol Biol. 2001; Chapter 8(Unit 8):3. [PubMed: 18265275]

53. Looke M, Kristjuhan K, Kristjuhan A. Extraction of genomic DNA from yeasts for PCR-based applications. Biotechniques. 2011; 50:325–328. [PubMed: 21548894]

54. Chase T Jr, Shaw E. p-Nitrophenyl-p′-guanidinobenzoate HCl: a new active site titrant for trypsin. Biochem Biophys Res Commun. 1967; 29:508–514. [PubMed: 16496527]

55. Lees JG, Miles AJ, Wien F, Wallace BA. A reference database for circular dichroism spectroscopy covering fold and secondary structure space. Bioinformatics. 2006; 22:1955–1962. [PubMed: 16787970]

56. Horovitz A, Rigbi M. Protein-protein interactions: additivity of the free energies of association of amino acid residues. J Theor Biol. 1985; 116:149–159. [PubMed: 3900586]

Summary statement

Cancer is a leading cause of morbidity and mortality worldwide. The results presented here pave the way to develop new therapies targeting mesotrypsin, an enzyme that contributes to progression and metastasis of lung, prostate, breast, and pancreatic cancers.
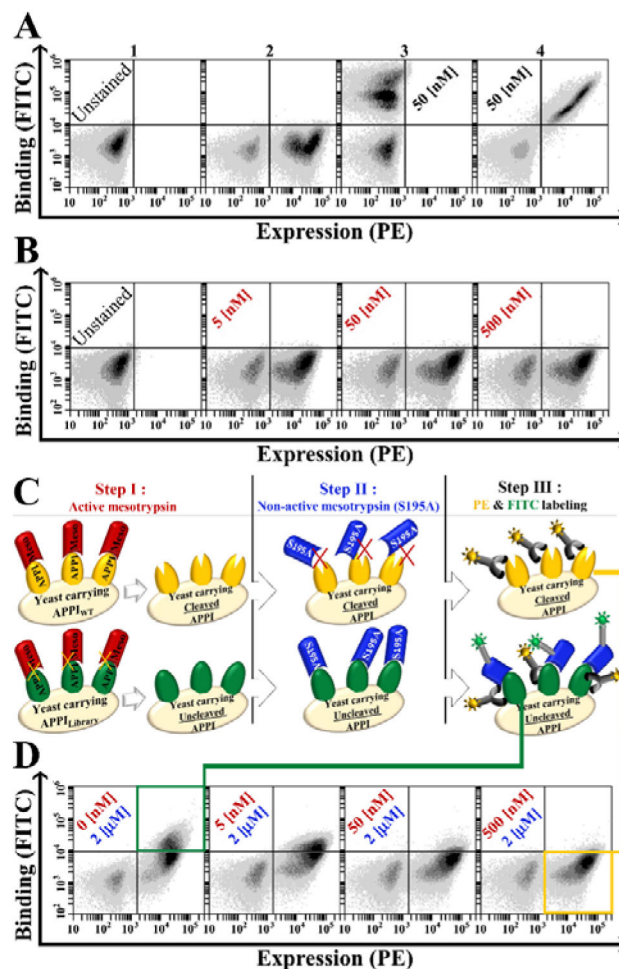
Figure 1. Yeast surface displayed APPI$_{WT}$ is cleaved by active mesotrypsin but detected by catalytically inactive mesotrypsin-S195A

(**A**) Dual-color flow cytometric expression and folding analysis. APPI expression is shown on the X-axis and binding of APPI to bovine-trypsin (50 nM) on the Y-axis. Subpanels 1, 2, 3 and 4 represent unstained, PE-labeled expression, FITC-labeled binding and dual-labeled cells (demonstrating expression and binding, respectively). (**B**) APPI$_{WT}$ is not detected by active mesotrypsin. Panel *B* shows dual-labeled cells as in panel *A*, after exposure to different concentrations of FITC-labeled active mesotrypsin (in red). (**C**) General scheme of the 'triple staining method' for detection of residual uncleaved APPI by FITC-labeled catalytically inactive mesotrypsin-S195A after preincubation of cells with active mesotrypsin. (**D**) Intact APPI is detected by mesotrypsin-S195A. Panel *D* shows dual-labeled cells, as in panel *B*, after stepwise exposure to unlabeled active mesotrypsin (in red) followed by FITC-labeled mesotrypsin-S195A (in blue). Preincubation with increasing concentrations of active mesotrypsin correlated with the loss of the FITC signal, suggesting cleavage of surface-displayed APPI$_{WT}$ by active mesotrypsin. For all panels, the surface expression of APPI was detected by using a primary antibody against the C-terminal c-Myc tag and a PE-labeled secondary antibody, while binding to APPI was detected by a biotinylated target (bovine trypsin or mesotrypsin) and FITC-labeled streptavidin. Non-

induced cells are shown in the bottom left quadrant of each plot. FITC- and PE-positive clones (green square) demonstrate resistant clones and FITC-negative PE-positive clones (yellow square) demonstrate cleaved clones.
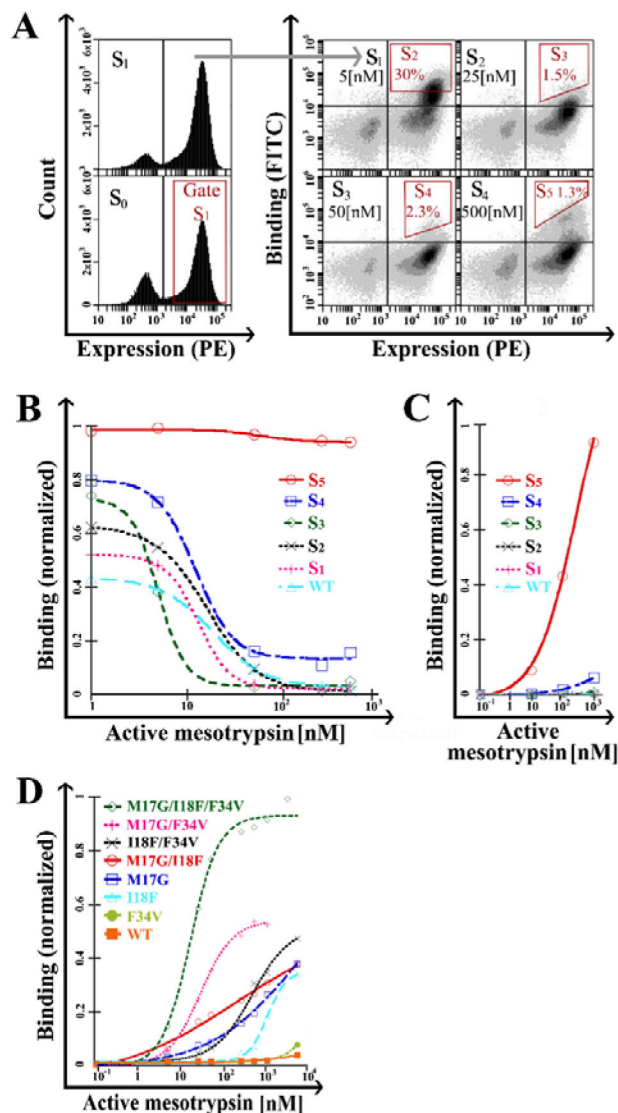
Figure 2. Identification of APPI clones with improved resistance to cleavage
(**A**) Stability maturation of the APPI library. FACS of single or dual-labeled cell populations for expression (S0 and S1) or both expression and binding (S1 to S5). The expressed population of APPI variants was sorted (S0), and the expression of the library was tested after enrichment (S1). Next, each cycle of stability maturation (S2 to S5) was performed with elevated concentrations of active mesotrypsin (as noted in the upper right quadrant of each plot) and a fixed concentration of inactive mesotrypsin (2 μM). Sorting gates are marked in red. (**B**) 'Triple staining' and (**C**) 'double staining' analysis of cell populations from library maturation cycles. (**D**) 'Double staining' analysis of cells expressing M17G, I18F, F34V and combination variants. A leftward shift in the sigmoid shape indicates a higher affinity, whereas a higher binding signal under saturating conditions indicates higher proteolytic stability. In panels *B–D*, the Y-axis represents mean fluorescence intensity normalization of binding to expression. Data was analyzed using KaleidaGraph software, with a sigmoidal curve fit. For all panels, the surface expression of APPI was detected by

using a primary antibody against the C-terminal c-Myc tag and a PE-labeled secondary antibody, while binding to APPI was detected by biotinylated mesotrypsin and FITC-labeled streptavidin.
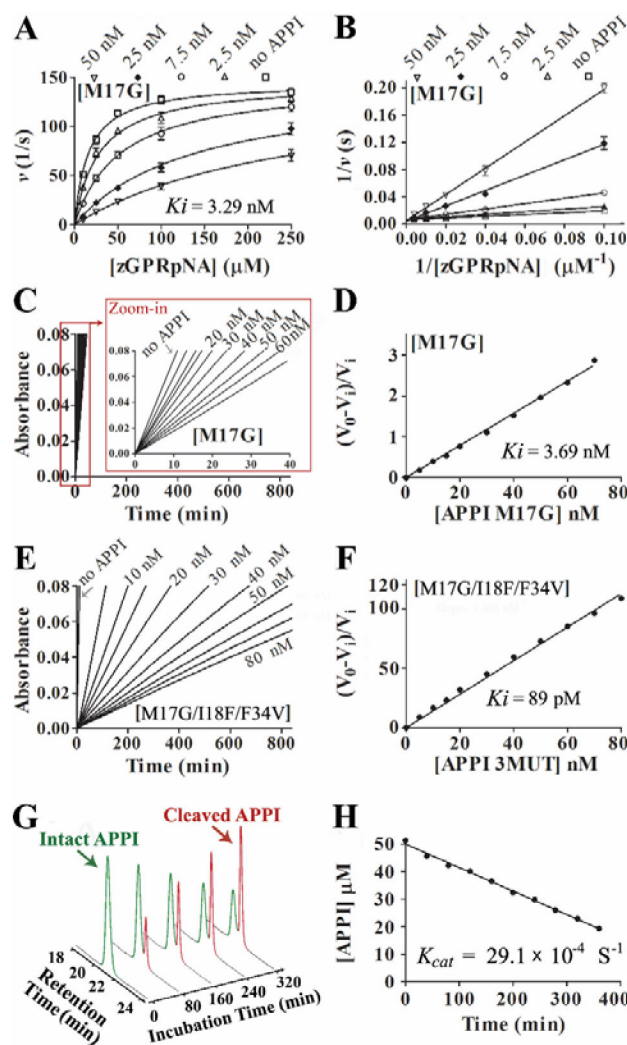
Figure 3. Kinetics of mesotrypsin inhibition by APPI and hydrolysis of APPI by mesotrypsin

(**A**) Competitive patterns of mesotrypsin inhibition by $APPI_{M17G}$. Mesotrypsin cleavage of peptide substrate Z-GPR-pNA is competitively inhibited by $APPI_{M17G}$. (**B**) The Lineweaver-Burk double reciprocal transform of the data used in panel *A*. The APPI (inhibitor) concentration is given at the top of each plot; the mesotrypsin concentration was 0.25 nM. Data was fitted globally to the competitive inhibition equation using Prism, GraphPad Software. (**C, E**) Slow, tight binding inhibition of mesotrypsin by APPI variants. Steady-state equilibrium for the reactions of $APPI_{M17G}$ (*C*) and $APPI_{M17G/I18F/F34V}$ (*E*) with various concentrations of APPI and 145 μM of peptide substrate Z-GPR-pNA. (**D, F**) A re-plot of slopes (V_0 and V_i) calculated from the binding curves shown in panels *C* and *E*, respectively, where V_0 is the uninhibited rate and V_i is the rate in the presence of inhibitor, which allows calculation of K_i using eq. 2 (as described in *SI Materials and Methods* under "Inhibition studies"). (**G**) Kinetics of $APPI_{M17G/I18F/F34V}$ hydrolysis by mesotrypsin. Representative HPLC chromatograms are shown from a time course of $APPI_{M17G/I18F/F34V}$ hydrolysis by mesotrypsin. Green and red peaks represent intact and cleaved inhibitor, respectively. (**H**) Initial rate of hydrolysis, from which k_{cat} is calculated. Disappearance of

intact $APPI_{M17G/I18F/F34V}$ was quantified by integration of the HPLC peak in a time course that is illustrated in panel *G*. Hydrolysis reaction contained 50 μM of $APPI_{M17G/I18F/F34V}$ and 2.5 μM of enzyme.
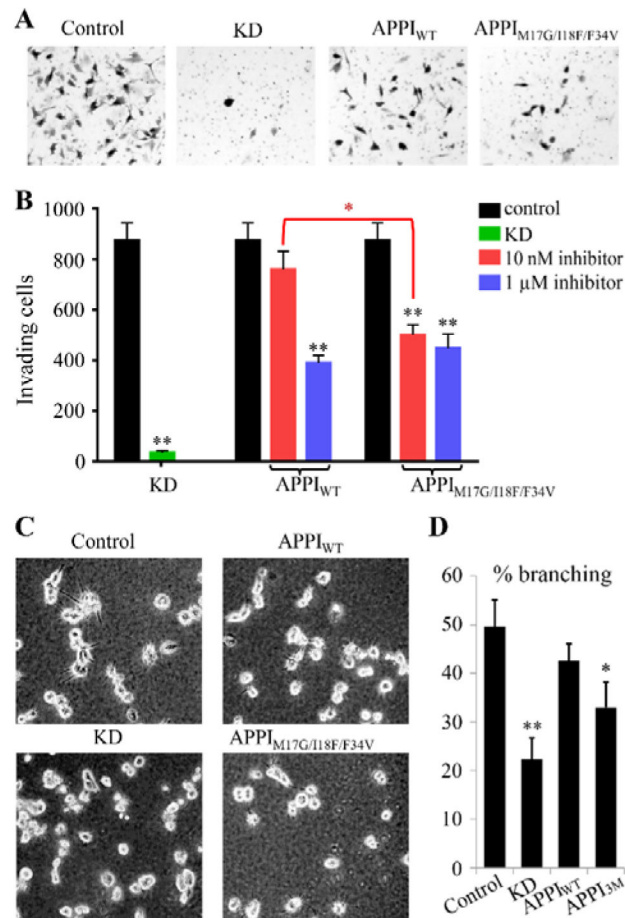
Figure 4. Enhanced potency of APPI$_{M17G/I18F/F34V}$ for inhibition of prostate cancer cell invasiveness

(**A,B**) In Matrigel invasion assays, shRNA knockdown (KD) of *PRSS3* or treatment with inhibitors APPI$_{WT}$ or APPI$_{M17G/I18F/F34V}$ led to reductions in PC3-M cellular invasion compared to control cells. (**A**) Images are shown for representative fields from stained invasion filters for (left to right) control cells, cells with *PRSS3* knockdown (KD), cells treated with 10 nM APPI$_{WT}$, and cells treated with 10 nM APPI$_{M17G/I18F/F34V}$. (**B**) Bar graph shows means and S.E.M. for quadruplicate biological replicates. Black bars represent control cell samples, green bar represents cells with *PRSS3* knockdown (KD), red bars represent cells treated with 10 nM inhibitor (APPI$_{WT}$ or APPI$_{M17G/I18F/F34V}$ as indicated), and blue bars represent cells treated with 1 μM inhibitor (APPI$_{WT}$ or APPI$_{M17G/I18F/F34V}$ as indicated). (**C,D**) In Matrigel 3D cell culture assays, shRNA knockdown of *PRSS3* (KD) or treatment with 100 nM APPI$_{M17G/I18F/F34V}$ (indicated as APPI$_{3M}$ in panel *D*), but not with APPI$_{WT}$, led to a significant reduction in the invasive branching morphology of PC3-M cells compared to control cells. (**C**) Images are shown for representative fields in 3D cultures for control cells, cells with *PRSS3* knockdown (KD), cells treated with 100 nM APPI$_{WT}$, and cells treated with 100 nM APPI$_{M17G/I18F/F34V}$, as indicated. (**D**) Bar graphs shows means and S.E.M. for quadruplicate biological replicates. **P<0.005 for t-test comparisons of indicated conditions versus control. *P = 0.02 for t-test comparison of 10 nM treatment

conditions for APPI$_{WT}$ *vs.* APPI$_{M17G/I18F/F34V}$ in panel *B; P* = 0.034 for t-test comparison of APPI$_{M17G/I18F/F34V}$ (APPI$_{3M}$) *vs.* control in panel *D.*
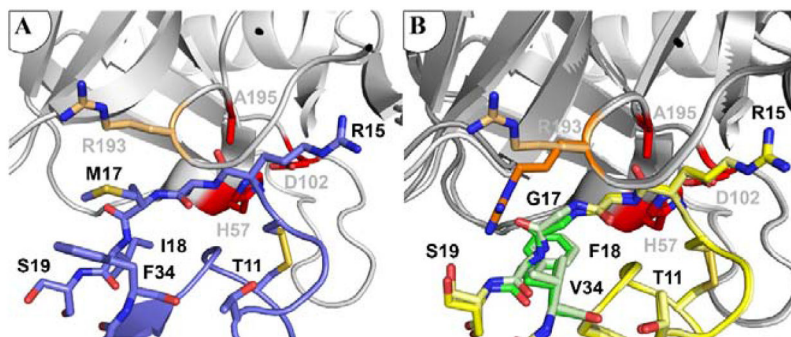
Figure 5. Mesotrypsin Arg-193 adopts multiple conformations in the complex with APPI$_{M17G/I18F/F34V}$

(**A**) Arg-193 conformation is constrained by interaction with APPI Met-17 in the mesotrypsin complex with APPI$_{WT}$. Mesotrypsin is shown in *gray* with catalytic triad residues in *red*, and the Arg-193 side chain rendered as *light orange sticks*; APPI$_{WT}$ is shown in *blue* (PDB entry: 3L33). (**B**) In complex with APPI$_{M17G/I18F/F34V}$, mesotrypsin Arg-193 is found in different conformations in the two copies of the structure in the asymmetric unit of the crystal, which here are shown superposed. Mesotrypsin is shown in *gray*, with catalytic triad residues in *red*; APPI$_{M17G/I18F/F34V}$ is shown in *yellow*, with mutated residues in *green*. The distinct 'up' and 'down' conformations of Arg-193 are illustrated in *light* and *dark orange*, respectively.
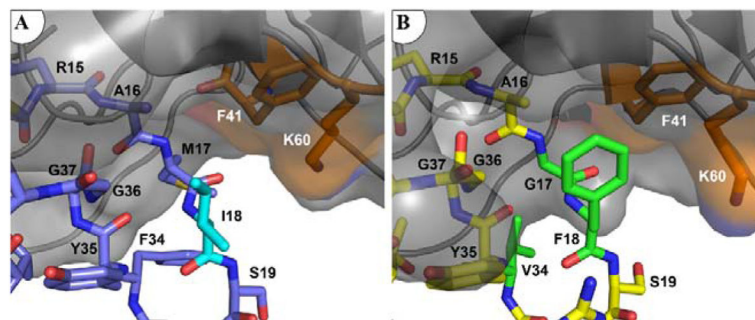
Figure 6. APPI$_{M17G/I18F/F34V}$ displays improved complementarity with the mesotrypsin S$_3'$ subsite

(**A**) APPI$_{WT}$ shows limited interactions with the mesotrypsin S$_3'$ subsite. Mesotrypsin cartoon and surface are shown in *gray*, with Phe-41 and Lys-60 in *orange*; APPI$_{WT}$ is shown in *blue*, with Ile-18 in *cyan* (PDB entry: 3L33). (**B**) Phe-18 of APPI$_{M17G/I18F/F34V}$ forms hydrophobic, ring-stacking, and amino-aromatic interactions with mesotrypsin Phe-41 and Lys-60 residues. Mesotrypsin is rendered and colored as above, with APPI$_{M17G/I18F/F34V}$ in *yellow* and mutated residues in *green*.
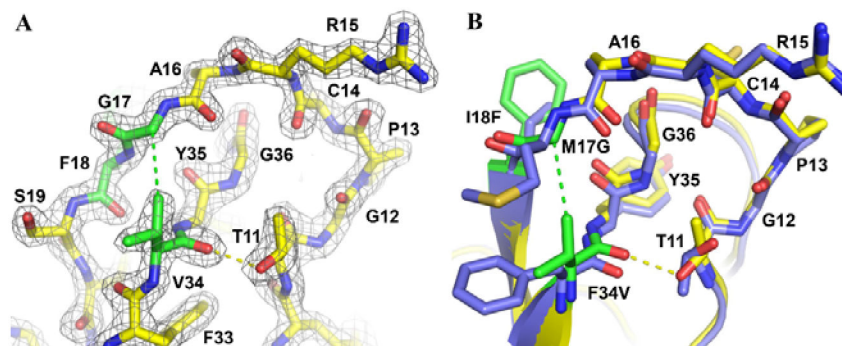
Figure 7. Enhanced intramolecular stabilizing features of APPI$_{M17G/I18F/F34V}$

The structure of APPI$_{M17G/I18F/F34V}$ bound to mesotrypsin reveals a new hydrophobic contact between Val-34 C$_{\gamma 1}$ and Gly-17 C$_{\alpha}$ (*green dashed line*) and a new H-bond between Val-34 O and Thr-11 OH (*yellow dashed line*). (**A**) 2F$_o$-F$_c$ density map is shown contoured at 2.0σ. APPI$_{M17G/I18F/F34V}$ is shown in *yellow*, with mutated residues in *green*. (**B**) APPI$_{M17G/I18F/F34V}$ is colored as above, superimposed upon APPI$_{WT}$ in *blue* to highlight small shifts in backbone positions. Thr-11 adopts a different rotamer conformation to facilitate formation of the H-bond.

Table 1

Kinetic constants of mesotrypsin with APPI variants

Inhibitor	K_i (M)[‡]	K_i (fold)	$K_{cat}(s^{-1})$[‡]	Turnover time (s)[‡]	Turnover time (fold)
APPI-WT	*$(1.31\pm0.17)\times10^{-7}$	1	$(35.6\pm2.3)\times10^{-3}$	28.1 ± 1.8	1
APPI-F34V	*$(5.01\pm0.46)\times10^{-8}$	2.6	$(16.1\pm1.6)\times10^{-3}$	62.4 ± 4.3	2.2
APPI-M17G	**3.69×10^{-9}	34.8			
APPI-M17G	*$(3.29\pm0.25)\times10^{-9}$	39.8	$(15.6\pm1.5)\times10^{-3}$	64.3 ± 6.4	2.3
APPI-118F	*$(3.29\pm0.21)\times10^{-9}$	39.8	$(10.4\pm0.9)\times10^{-3}$	96.5 ± 8.2	3.4
APPI-118F/F34V	**$(3.3\pm0.07)\times10^{-9}$	39.8	$(5.35\pm0.2)\times10^{-3}$	187.1 ± 7.7	6.6
APPI-M17G/F34V	**$(1.40\pm0.11)\times10^{-9}$	93.6	$(37.1\pm1.4)\times10^{-4}$	270.0 ± 10.1	9.6
APPI-M17G/118F	**$(45.25\pm0.36)\times10^{-11}$	290	$(29.1\pm0.6)\times10^{-4}$	344.0 ± 7.6	12.2
APPI-M17G/118F/F34V	**$(89.8\pm0.23)\times10^{-12}$	1459	$(4.29\pm0.3)\times10^{-4}$	2336.7 ± 140.0	83

*and**
represent fitted to Equations 1 and 2 (see SI), respectively.

[‡]Values arc means ± SD.

Table 2

The inhibitor specificity of APPI-M17G/118F/F34V towards a range of human serine proteases

Inhibitor	K_i for mesotrypsin $(M)^{†‡}$	K_i for kallikrein-6 $(M)^{†‡}$	K_i for cationic trypsin $(M)^{†‡}$	K_i for anionic trypsin $(M)^{†‡}$	K_i for FXIa $(M)^{†‡}$
APPI-WT	$(1.31\pm0.17)\times10^{-7}$	$(2.23\pm0.18)\times10^{-9}$	$(6.27\pm1.01)\times10^{-12}$	$(1.74\pm0.05)\times10^{-12}$	$(4.1\pm0.14)\times10^{-10}$
APPI-M17G/118F/F34V	$(89.8\pm0.23)\times10^{-12}$	$(1.09\pm0.12)\times10^{-9}$	$(4.96\pm0.25)\times10^{-12}$	$(1.47\pm0.02)\times10^{-12}$	$(9.84\pm0.32)\times10^{-8}$
K_i (fold)	1459	2.04	1.3	1.18	4.16×10^{-3}
Specificity $\left(\dfrac{K_i\ (fold)\ \text{for Mesotrypsin}}{K_i\ (fold)\ \text{for protease } X}\right)$	1	715	1122	1236	350000

†Values are means ± SD.